

UNIVERSIDADE ESTADUAL DE CAMPINAS  
SISTEMA DE BIBLIOTECAS DA UNICAMP  
REPOSITÓRIO DA PRODUÇÃO CIENTÍFICA E INTELECTUAL DA UNICAMP

**Versão do arquivo anexado / Version of attached file:**

Versão do Editor / Published Version

**Mais informações no site da editora / Further information on publisher's website:**

<https://link.springer.com/article/0.1007/s13538-012-0099-5>

**DOI: 10.1007/s13538-012-0099-5**

**Direitos autorais / Publisher's copyright statement:**

©2012 by Springer. All rights reserved.

DIRETORIA DE TRATAMENTO DA INFORMAÇÃO

Cidade Universitária Zeferino Vaz Barão Geraldo

CEP 13083-970 – Campinas SP

Fone: (19) 3521-6493

<http://www.repositorio.unicamp.br>

# Total Hadronic Cross-Section Data and the Froissart–Martin Bound

Daniel Almeida Fagundes · Marcio José Menon ·  
Paulo Victor Recchia Gomes Silva

Received: 22 March 2012 / Published online: 9 October 2012  
© Sociedade Brasileira de Física 2012

**Abstract** The energy dependence of the total hadronic cross section at high energies is investigated with focus on the recent experimental result by the Total Elastic and Diffractive Cross-section Measurement Collaboration at 7 TeV and the Froissart–Martin bound. On the basis of a class of analytical parametrization with the exponent  $\gamma$  in the leading logarithm contribution as a free parameter, different variants of fits to pp and  $\bar{p}p$  total cross-section data above 5 GeV are developed. Two ensembles are considered, the first comprising data up to 1.8 TeV and the second also including the data collected at 7 TeV. We show that in all fit variants applied to the first ensemble, the exponent is statistically consistent with  $\gamma = 2$ . Applied to the second ensemble, however, the same variants yield  $\gamma$  values above 2, a result already obtained in two other analysis, by Amaldi et al. and by the UA4/2 Collaboration. As recently discussed by Azimov, this faster-than-squared-logarithm rise does not necessarily violate unitarity. Our results suggest that the energy dependence of the hadronic total cross section at high energies still constitutes an open problem.

**Keywords** High-energy hadron interactions · Total cross section · Asymptotic problems and properties

## 1 Introduction

### 1.1 General Aspects

High-energy particle collisions constitute the main experimental tool in the investigation of the inner structure of matter. In particle physics, high-energy usually means center-of-mass energies above  $10 m_p \sim 10$  GeV, where  $m_p$  is the proton mass<sup>1</sup> [1]. Presently, for particle–particle and antiparticle–particle collisions, the highest energies reached in accelerators concern proton–proton (pp) and antiproton–proton ( $\bar{p}p$ ) interactions, corresponding to 7 and  $\sim 2$  TeV, respectively. These hadronic processes are expected to be described by the quantum chromodynamics (QCD), the non-Abelian gauge field theory of the strong interactions [2].

As a non-Abelian theory, the gluons (the field quanta) themselves carry a color charge and can therefore interact with other gluons.<sup>2</sup> The dynamical consequence is a running coupling constant  $\alpha_s$ ; the color charge is small at short distances and large at large distances, leading to two different regimes named asymptotic freedom and confinement, respectively [1–3]. In hadron–hadron collisions, these regimes correspond to two sectors that have been known as hard scattering (small distances and large values of the momentum transfer) and soft scattering (large distances and small values of the momentum transfer). The confinement

D. A. Fagundes · M. J. Menon · P. V. R. G. Silva (✉)  
Instituto de Física Gleb Wataghin, Universidade Estadual de  
Campinas—UNICAMP, 13083-859 Campinas,  
São Paulo, Brazil  
e-mail: precchia@ifi.unicamp.br

M. J. Menon  
e-mail: menon@ifi.unicamp.br

<sup>1</sup>As usual, in high-energy physics, we adopt the system of units in which  $c = \hbar = 1$ . Typical units of energy are 1 GeV =  $10^9$  eV and 1 TeV =  $10^{12}$  eV.

<sup>2</sup>This property contrasts with QED since photons do not have electric charge.

barrier, where  $\alpha_s \sim 1$ , is typical of distances of the order of 1 fm and therefore “peripheral” hadronic collisions correspond to the soft sector.

The great triumph of QCD concerns the perturbative techniques, successfully applied in the hard sector [4]. By contrast, soft interactions, characterized by small values of the momentum transfer, cannot be treated through these techniques due to the rise of the coupling constant as the momentum transfer decreases. As a consequence, soft physics demands first principles and nonperturbative approaches, which means the nontrivial investigation of the vacuum structure, intricate Monte Carlo simulations, and complex analytic formalisms [5]. However, despite the success of nonperturbative QCD in the investigation of the static hadronic properties (bound states), a formal approach to *soft scattering states*, based on first principles and without model assumptions, is still missing [6, 7] and that implies in some fundamental problems.

Soft scattering embodies elastic collisions and diffraction dissociation (single and double) [6] and here comes one of the striking features of QCD: elastic scattering, the simplest kinematic collision process, just constitutes one of the greatest dynamic problems for the theory of the strong interactions. In this respect, the optical theorem [8] plays a crucial role since it connects the forward *elastic* scattering amplitude with the most important physical quantity characterizing a collision process, namely, the total cross section [6, 7]. Therefore, the lack of a pure QCD result for the elastic amplitude puts serious limits in the theoretical investigation of the total hadronic cross section. On the other hand, and more important for our purposes, experimental information on the behavior of the total cross section may, in principle, be used as an input providing new insights in the development of the theory in the soft sector (the inverse problem), at least in what concerns the forward elastic scattering amplitude.

Operationally, the total cross section is defined by [6, 9]

$$\sigma_{\text{tot}} = \frac{N_{\text{el}} + N_{\text{inel}}}{\mathcal{L}},$$

where  $\mathcal{L}$  is the luminosity (flux per unit area) and  $N_{\text{el}}$  and  $N_{\text{inel}}$  are the rate of elastic and inelastic interactions, respectively (scattered fluxes). From the definition, two interpretations emerge for  $\sigma_{\text{tot}}$ , one is statistical, as a probability of interaction (ratio between incident and scattered particles) and the other is geometrical, as an effective area of interaction, usually measured in millibarn for hadronic scattering.

Experiments indicate that at lower energies, below  $\sim 2$  GeV,  $\sigma_{\text{tot}}$  is characterized by narrow peaks, caused

by the formation of resonances (bound states). As the energy increases, reaching the scattering region,  $\sigma_{\text{tot}}$  decreases very slowly up to  $\sim 20$  GeV and then starts to grow smoothly and monotonically (without bumps or dips), as illustrated by the experimental points in Fig. 1, in the case of pp and  $\bar{p}p$  scattering (see also Fig. 41.10 in [10]). The energy dependence of  $\sigma_{\text{tot}}$  is therefore a crucial point since, above the resonance region, it is directly related to the soft sector (optical theorem) giving information on the dynamics of the elastic interaction [6, 7].

## 1.2 Purposes and Goals of the Paper

Although the rise of the total hadron–hadron cross sections at high energies is an experimental fact, the exact energy dependence involved has been a long-standing problem. Several phenomenological models, with distinct physical pictures and good descriptions of the available data, make different asymptotic predictions [9, 11, 12] and the only general, formal, widely accepted result is the well-known Froissart–Martin (FM) bound [13, 14]

$$\sigma_{\text{tot}}(s) \leq c \ln^2 \frac{s}{s_0}, \quad (1)$$

where  $s$  is the squared center-of-mass energy,  $s_0$  is a constant, and a bound on the first term on the right-hand side,

$$c \leq \pi/m_\pi^2 \approx 60 \text{ mb}, \quad (2)$$

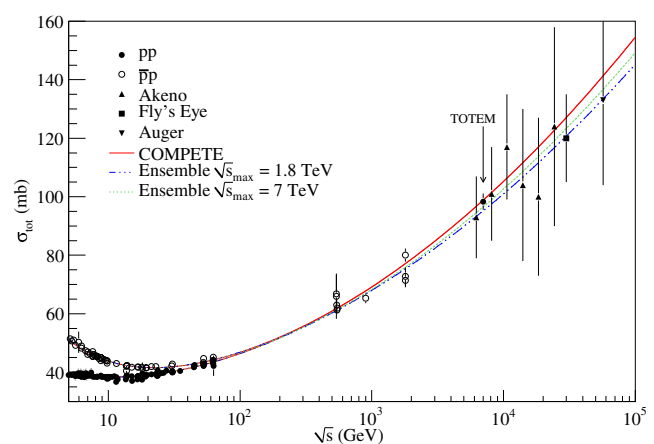


**Fig. 1** (Color online) Comparison between experimental data and fit results. The *dot-dashed* and *dotted* lines display the results of the direct fit of method 1 applied to the  $\sqrt{s}_{\text{max}} = 1.8$  TeV and  $\sqrt{s}_{\text{max}} = 7$  TeV ensembles, respectively. The *solid* line is the fit obtained by the COMPETE Collaboration. Numerical information are displayed in Tables 1 (second and third columns) and 2 (second column)

has been obtained by Lukaszuk and Martin [15]. Even recently, the foundations of this key result in soft hadronic physics have been discussed in the literature [16–18]. In particular, Azimov has presented a short critical review on the assumptions supporting the derivation of the bound [18].

Even depending on the unknown squared mass scale  $s_0$ , the numerical values associated with the FM bound lie far above the existing data for the total cross section. For example, for  $s_0$  in the interval 1–50 GeV<sup>2</sup>, the bound in (1–2) at 1 TeV is of order of 10 b, much larger than the 100-mb cross sections typically found in experiments at the highest energies. However, the bound also comprises a maximum rate of rise for the cross section with the energy, namely, the squared logarithm behavior at the asymptotic energy region and that is the point we are interested in here. Different dependencies have been extensively tested and discussed in the literature, specially in the context of amplitude analyses, which are characterized by analytical parametrization for the total cross section and fits to forward data. The most common functional forms employed in the highest energy region include different combinations of constant, linear/quadratic logarithm dependencies and  $s$  power laws, as discussed, for example, in [19–28] and references therein. Nonetheless, like the case of specific phenomenological models [9, 11, 12], these analyses present good descriptions of the available data with different functional forms and hence offer different physical pictures.

New results from the CERN Large Hadron Collider (LHC) and new estimates from the Pierre Auger Observatory for the proton–proton total cross sections are expected to shed light on the subject, not only by selecting phenomenological models/pictures but also by providing information on the degree of possible saturation of the bound in terms of the energy dependence of the cross section. In fact, at 7 TeV, the first result for the total cross section by the Total Elastic and Diffractive Cross-section Measurement (TOTEM) Collaboration, a luminosity-dependent measurement [29], indicates consistency with a  $\ln^2 s$  dependence, as predicted 10 years ago by the parametrization that was ranked highest by the Computerized Models and Parameter Evaluation for Theory and Experiment (COMPETE) Collaboration [24, 25], also quoted in the *Review of Particle Physics* by the Particle Data Group [10]. Therefore, these results favor the maximum increase rate allowed by the bound.

By contrast, at least two previous almost-model-independent analyses, based on data ensembles at lower energies, have indicated that the exponent in the logarithm may be somewhat larger than 2 [30, 31].

Moreover, on the theoretical side, as recently discussed by Azimov [18], it is not obvious if Martin's derivation, in the context of axiomatic local quantum field theory, can be directly applied to hadronic processes. Formal arguments suggest that the total cross section could grow faster than  $\ln^2 s$ . A recent result from lattice QCD [32] indicates a universal asymptotic squared logarithm dependence for the hadronic total cross section. That conclusion nonetheless rests on specific assumptions and is hence neither unique or exclusive.

In view of these facts, taking into account the TOTEM result and considering the exponent of the logarithm as a free fit parameter, the following questions arise. Is the  $\ln^2 s$  dependence an unique solution describing the asymptotic rise of the total cross section? Could the data be statistically described by another solution, rising faster (or slower) than  $\ln^2 s$ ? To address these questions is the goal of this work.

For this purpose, we shall revisit the analytical parametrization introduced by Amaldi et al. in the 1970s [30] and also employed by the UA4/2 Collaboration in the 1990s [31], characterized by Reggeon contributions at low energies and a leading contribution at high energies parametrized by a power law in  $\ln s$ , with the real exponent  $\gamma$  as a free parameter. As will be recalled along the text, the two analyses cover different energy intervals and led to an exponent exceeding 2. For future reference, we note that the above-mentioned highest ranking parametrization, obtained by the COMPETE Collaboration [24, 25], can be regarded as a particular instance of this parametrization in which the exponent was fixed at  $\gamma = 2$ .

All these works developed simultaneous fits to  $\sigma_{\text{tot}}$  and the  $\rho$  parameter (ratio between the real and imaginary parts of the forward amplitude). Here, for reasons to be discussed in detail, we shall analyze only the  $\sigma_{\text{tot}}$  data, from pp and  $\bar{p}p$  scattering above  $\sqrt{s} = 5$  GeV. In order to investigate the effect of the recent experimental result for the pp total cross sections by the TOTEM Collaboration, we first consider all the previous existing data, covering the region up to 1.8 TeV and then add to the ensemble the data at 7 TeV. We choose two different initial values for the free fit parameters and six fitting variants. We show that, with data up to 1.8 TeV, the real exponent in the logarithm term is statistically consistent with  $\gamma = 2$ , as predicted by the COMPETE Collaboration. However, with the addition of the data at 7 TeV, the fits indicate exponents larger than 2 in all cases investigated.

The manuscript is organized as follows: In Section 2, we introduce the analytical parametrization, followed by some comments on its applicability and a critical discussion on the selected data ensemble. In Section 3,

we present the fit procedures, variants, and results. The conclusions and some final remarks are the contents of Section 4.

## 2 Analytical Parametrization and Data Ensemble

### 2.1 Analytical Parametrization and Previous Results

The class of analytical parametrization [30, 31] consists of two components for the total hadronic cross section associated with low- ( $L$ ) and high-energy ( $H$ ) contributions:

$$\sigma_{\text{tot}}(s) = \sigma_{\text{LE}}(s) + \sigma_{\text{HE}}(s). \quad (3)$$

The first term accounts for the decreasing of the total cross section and the differences between particle–particle and particle–antiparticle scattering at low energies and is expressed by

$$\sigma_{\text{LE}}(s) = a_1 \left[ \frac{s}{s_l} \right]^{-b_1} + \tau a_2 \left[ \frac{s}{s_l} \right]^{-b_2}, \quad (4)$$

where  $s_l = 1 \text{ GeV}^2$  (fixed) while  $a_1$ ,  $b_1$ ,  $a_2$ , and  $b_2$  are free fit parameters, and

$$\tau = \begin{cases} -1 & \text{for particle–particle} \\ +1 & \text{for antiparticle–particle.} \end{cases}$$

The second term accounts for the rising of the cross section at higher energies and is given by

$$\sigma_{\text{HE}}(s) = \alpha + \beta \ln^\gamma \frac{s}{s_h}, \quad (5)$$

where  $\alpha$ ,  $\beta$ ,  $\gamma$ , and  $s_h$  are real free parameters. For further discussion, let us briefly recall some formal aspects and previous results associated with this class of parametrization.

In the context of the Regge–Gribov theory, all terms in (4) and (5) have specific physical interpretations, namely, Reggeon and Pomeron exchanges at low and high energy regions, respectively [25]. The Reggeons correspond to mesons resonances families with the adequate quantum numbers in the  $t$ -channel process and represented by trajectories interpolating the data on plots of spin  $J$  versus the square of their masses (Chew–Frautschi plot). In this case,  $b_1$  and  $b_2$  correspond to the intercept of the trajectories, and  $a_1$  and  $a_2$ , the Reggeon strengths (residues). For pp and  $\bar{p}p$  scattering,  $\sigma_{\text{LE}}$  is associated with two Reggeons, the first one with  $C = +1$  ( $a_2$  and  $f_2$  mesons' trajectories) and the second with  $C = -1$  ( $\rho$  and  $\omega$  mesons' trajectories), corresponding to  $\tau = +1$  and  $\tau = -1$ , respectively. The type of Pomeron contribution depends on the  $\gamma$  value. For  $\gamma = 1$ , the constant plus  $\ln s$  terms correspond to

a double pole at  $J = 1$ , and for  $\gamma = 2$ , a triple pole (expressed by  $\ln^2 s$ ,  $\ln s$ , and the constant terms). Up to our knowledge, the case of real exponent and  $0 < \gamma < 2$  corresponds to a strong-coupling scenario (critical Pomeron) [33, 34] and a fractional power,  $\gamma = 3/2$  (in general  $1 < \gamma < 2$ ), is indicated by the mini-jet QCD model with infrared gluon resummation [35, 36].

As commented before, the above parametrization has been introduced by Amaldi et al. [30], with  $\sigma_{\text{LE}}$  expressed as a function of the lab energy,  $\sigma_{\text{HE}}$  as function of  $s$ , and with a fixed scale constant  $s_h = 1 \text{ GeV}^2$ . Simultaneous fits to  $\sigma_{\text{tot}}$  and  $\rho$  data (via dispersion relations) from pp and  $\bar{p}p$  scattering in the interval  $5 < \sqrt{s} \leq 62 \text{ GeV}$  have led to the result

$$\gamma = 2.10 \pm 0.10.$$

The same functional form was subsequently used by the UA4/2 Collaboration [31]. Simultaneous fits to  $\sigma_{\text{tot}}$  and  $\rho$  data from pp and  $\bar{p}p$  scattering in a larger interval,  $5 < \sqrt{s} \leq 546 \text{ GeV}$ , have yielded the result

$$\gamma = 2.25^{+0.35}_{-0.31}.$$

More recently, the COMPETE Collaboration has carried out a detailed and extensive study on possible analytic parametrizations including all measured  $\sigma_{\text{tot}}$  and  $\rho$  data from pp,  $\bar{p}p$ , meson-p scattering, among other processes, at  $\sqrt{s} \geq 4 \text{ GeV}$  and  $\bar{p}p$  data up to 1.8 TeV [24, 25]. Different aspects of fit qualities have been considered in a ranking procedure with the same  $\sigma_{\text{LE}}$  structure and  $\sigma_{\text{HE}}$  parametrized either with  $\gamma = 1$  or  $\gamma = 2$  and the constant term. The parametrization with  $\gamma = 2$  was ranked the highest. As commented before, the predictions from this analysis, carried out 10 years ago, indicate consistency with the TOTEM result at 7 TeV and therefore agree with the saturation of the squared logarithm dependence in the FM bound.

### 2.2 Data Ensemble and Critical Comments

Two aspects of our choice of data ensemble deserve special attention. One aspect concerns the reactions and the other the physical quantities to be investigated, as discussed in what follows.

First, the squared logarithm dependence in the FM bound is an asymptotic result, and the parametrization (3–5) covers particle–particle and particle–antiparticle interactions. For those reasons, we shall consider only the cases with the *highest energy interval in terms of available data*, namely, pp and  $\bar{p}p$  scattering. With

this restrictive choice, we do not take account of any constraint dictated by a supposed universal behavior, or data from other reactions in the region of intermediated and low energies, as for example the meson–proton cases. Following Amaldi et al. and the UA4/2 Collaboration, we focus our analysis on data at  $\sqrt{s} \geq 5 \text{ GeV}^2$ .

Second, as we have commented before, amplitude analyses of the growth of the total cross section include information on the  $\rho$  parameter, through dispersion relations (integral and/or derivatives forms), or the asymptotic prescriptions for crossing even and odd amplitudes (Phragmén-Lindelöf theorem) [37–39]. With the exponent  $\gamma$  as a real free fitting parameter, the integral dispersion relations demand numerical methods and therefore require a specific approach for error propagation from the uncertainty in the  $\gamma$  parameter. The use of prescriptions seems to us unjustified in the region of intermediate and low energy data, since they are asymptotic results [37]. By contrast, derivative dispersion relations allow an analytical approach and can be extended down to 4–5 GeV [40, 41] or even below (above the physical threshold) in the form of a double infinite series [42, 43] or a single series [44]. However, and that is a crucial point in this work, we shall not consider simultaneous fits to total cross-section data and  $\rho$  information for the six reasons that follows:

1. Strictly speaking, the  $\rho$  parameter is not a quantity with the same physical status as the total cross section since, in practice, it is evaluated as a free fit parameter in the Coulomb–nuclear interference region or inferred from analytical parametrization [38, 39].
2. As the energy grows, it becomes progressively more difficult to determine  $\rho$  [38, 39] and therefore the associated uncertainty, as can be easily seen in plots of this parameter in terms of the energy. Even the COMPETE Collaboration refers to the difficulty to adequately fit the  $\rho$  data from pp scattering [25].
3. Simultaneous fits to total cross-section data and  $\rho$  parameter demand the use of dispersion relations with one subtraction [45, 46] and therefore one more parameter, the subtraction constant. However, this constant does not have a physical interpretation, contrasting therefore with all the parameters in the  $\sigma_{\text{tot}}$  parametrization (shortly discussed in Section 2.1).
4. In data reductions, the correlation of the subtraction constant with all the other (physical) parameters affects the fit results at both low- and high-energy regions, as discussed in detail in [47]. As a consequence, the presence or the absence of the subtraction constant may lead to different results. In this respect, we note that, although referred to in [30], the value of the subtraction constant is not given (null or neglected?); in [31], its fit value is  $-57 \pm 4$  and it is neglected in the prescriptions or derivative dispersion relations used by the COMPETE Collaboration [24, 25]. It should also be noted that even the prediction of the  $\rho$  parameter from fits to total cross-section data is affected by the presence or absence of the subtraction constant [47, 48].
5. As recently demonstrated by Ferreira [49] and collaborators [50, 51] (see also [52]), the different slopes associated with the real and imaginary parts of the hadronic amplitude in the Coulomb–nuclear interference region affect the extracted value of the  $\rho$  parameter. This effect, however, has never been considered in the experimental procedures used in the  $\rho$  determination. The limited validity of the relative phase between Coulomb and nuclear amplitudes, used in the experimental procedures to determine  $\rho$ , has also been discussed by Kundrát et al. [53].
6. As a consequence of the above-mentioned effects and the increasing uncertainty in the  $\rho$  determination with the energy, any possible deviation from an analytical parametrization for the total cross section, dictated by the experimental data at the highest energies, may be hidden or lost. In other words, the inclusion of the  $\rho$  information may erroneously anchor the rise of the total cross section at the highest energies.

These six critical points suggest that, at the high-energy region, fits restricted to the total cross-section data may avoid the bias introduced by both the  $\rho$  parameter and the subtraction constant embodied in the dispersion relations. Therefore, although not being a usual procedure in amplitude analysis, we understand that to explore the possibility of focusing our fits only on the total cross-section data constitutes, at least, a valid strategy. For that reason, our data sample comprises only the pp and  $\bar{p}p$  total cross-section data above 5 GeV [10], including the special recent TOTEM result at 7 TeV [29].

Two points must be stressed in the analysis that follows: (1) we are concerned only with the rate of increase of the total cross section, not with the numerical value of the FM bound, and (2) our data ensemble is only a subset of the data employed in the global analysis by the COMPETE Collaboration.

### 3 Fitting Procedure, Variants, and Results

By means of a luminosity-dependent method, the TOTEM Collaboration has recently obtained for the pp total cross section at 7 TeV the value  $\sigma_{\text{tot}}^{\text{pp}} = 98.3 \pm 0.2^{\text{stat}} \pm 2.8^{\text{syst}}$  mb [29]. Our point here is to investigate the effect of this new data in the previous analytical fits covering the energy interval  $5 \text{ GeV} \leq \sqrt{s} \leq 1.8 \text{ TeV}$ , as was the case with the COMPETE Collaboration. Based on the results by Amaldi et al. and by the UA4/2 Collaboration, our strategy amounts to using the parametrization (3–5) to investigate possible deviations from  $\gamma = 2$ .

However, several aspects related to fitting procedure and the alternatives allowed by physical considerations or assumptions deserve investigation. The three main points are the following: (1) the nonlinearity of the fit demands a methodology for the choice of the initial (feedback) values of the free parameters [54]; (2) as commented in Section 2.1, in the theoretical context, the intercepts  $b_1$  and  $b_2$  are expected to be consistent with spectroscopic data (Chew–Frautschi plot); and (3) fixing  $b_1$  and  $b_2$  affects the fit results in both low- and high-energy regions, due to the correlation among the free parameters. In order to address these points, the following methodology and fit variants have been considered.

In all cases under study, we first consider the ensemble in the interval  $5 \text{ GeV} \leq \sqrt{s} \leq 1.8 \text{ TeV}$ , and after that, we include the data at 7 TeV from the TOTEM Collaboration. For easier reference, we will denote these two ensembles by  $\sqrt{s}_{\text{max}} = 1.8 \text{ TeV}$  and  $\sqrt{s}_{\text{max}} = 7 \text{ TeV}$ , respectively. In order to investigate the effects of different choices for the initial values of the free parameters, we have followed two alternative procedures, named method 1 and method 2:

#### Method 1

Since the highest rank result by the COMPETE Collaboration predicts a  $\ln^2 s$  dependence and is consistent with the TOTEM result at 7 TeV, we consider as a kind of orthodox choice to initialize our parametric set with the central values they have obtained in the simultaneous fit to  $\sigma_{\text{tot}}$  and  $\rho$  data, which includes pp and  $\bar{p}p$  in the interval  $5 \text{ GeV} \leq \sqrt{s} \leq 1.8 \text{ TeV}$  as a subset. The numerical values [10] are displayed in the second column of Table 1.

#### Method 2

Alternatively, we have chosen  $b_1 = b_2 = 0.5$  (average values for Reggeon intercepts),  $\gamma = 2$ ,  $a_1 = a_2 =$

$\alpha = 1 \text{ mb}$ ,  $s_h = 1 \text{ GeV}^2$ , and  $\beta = 50 \text{ mb}$  (simulating a saturation of the Lukaszuk–Martin bound [20]). The numerical values are displayed in the first column of Table 3.

The data reductions were carried out with the objects of the class TMinuit of the ROOT Framework (<http://root.cern.ch/drupal/>, <http://root.cern.ch/root/html/TMinuit.html>). A confidence level of  $\approx 68 \%$  (1 standard deviation) was adopted in all fits, so that the projection of the  $\chi^2$  distribution in  $(N + 1)$ -dimensional space ( $N =$  number of free fit parameters) has the probability of 68 % [54].

With both methods and the two ensembles, different variants were also considered. Sections 3.1 and 3.2 describe the variants and present the results obtained with methods 1 and 2, respectively, with the discussion of the results being deferred to Section 4.

#### 3.1 Method 1

##### 3.1.1 Results for the $\sqrt{s}_{\text{max}} = 1.8 \text{ TeV}$ Ensemble

We consider the cases and notation that follow. The numerical results and statistical information are displayed in Table 1.

##### Direct Fit:

Initialized with the COMPETE parameters and  $\gamma = 2$  (fixed). The first run of the MINUIT Code yields the  $\chi^2$  for that ensemble (second column of Table 1) and the final run gives the direct fit result for that ensemble (third column of Table 1).

**Variant 1 (V1):** Initialized with the direct fit parameters but now with the exponent  $\gamma$  as a free parameter (fourth column of Table 1).

**Variant 2 (V2):** Also initialized with the direct fit results. In this case, we consider  $\gamma = 2$  (fixed), and  $b_1$  and  $b_2$  were also fixed to the intercepts extracted from the spectroscopic data on the  $a_2/f_2$  and  $\rho/\omega$  mesons' trajectories, obtained by Luna et al., namely,  $b_1 = 0.452$  and  $b_2 = 0.558$  [55] (fifth column of Table 1).

**Variant 3 (V3):** Also initialized with the direct fit results. In this case, we consider  $\gamma$  free and  $b_1$  and  $b_2$  fixed as in variant 2 (sixth column of Table 1).

**Table 1** Results of method 1 for the  $\sqrt{s}_{\max} = 1.8$  TeV ensemble

	Initial values (COMPETE)	Direct fit	V1	V2	V3
$a_1$	$42.53 \pm 0.23$	$54.6 \pm 4.0$	$54.6 \pm 1.7$	$55.4 \pm 3.1$	$57.0 \pm 2.5$
$b_1$	$0.458 \pm 0.017$	$0.491 \pm 0.067$	$0.4907 \pm 0.0095$	0.452 (fixed)	0.452 (fixed)
$a_2$	$33.34 \pm 0.033$	$33.1 \pm 2.3$	$33.1 \pm 1.7$	$35.78 \pm 0.36$	$35.78 \pm 0.39$
$b_2$	$0.545 \pm 0.007$	$0.540 \pm 0.016$	$0.540 \pm 0.012$	0.558 (fixed)	0.558 (fixed)
$\alpha$	$35.45 \pm 0.48$	$34.2 \pm 2.5$	$34.19 \pm 0.24$	$32.14 \pm 0.99$	$31.38 \pm 0.98$
$\beta$	$0.308 \pm 0.010$	$0.264 \pm 0.029$	$0.263 \pm 0.018$	$0.245 \pm 0.018$	$0.180 \pm 0.062$
$\gamma$	2	2 (fixed)	$2.001 \pm 0.026$	2 (fixed)	$2.083 \pm 0.095$
$s_h$	$28.9 \pm 5.4$	$12 \pm 12$	$12.2 \pm 1.5$	$5.7 \pm 3.0$	$2.8 \pm 2.6$
DOF	156	156	155	158	157
$\chi^2/\text{DOF}$	1.02	0.931	0.937	0.929	0.934

Fit result from the COMPETE parameters as initial values, direct fit, and variants 1, 2, and 3 (initial values from the direct fit result), together with the statistical information: degrees of freedom (DOF) and reduced  $\chi^2$ . The parameters  $a_1$ ,  $a_2$ ,  $\alpha$ , and  $\beta$  are in millibarn,  $s_h$  is in gigaelectronvolt squared and  $b_1$ ,  $b_2$ , and  $\gamma$  are dimensionless

In terms of the initial values and data reductions, the following diagram summarizes the fitting procedures:

COMPETE results  $\rightarrow$  Direct Fit  $\rightarrow$   $\begin{cases} \text{Variant 1} \\ \text{Variant 2} \\ \text{Variant 3} \end{cases}$

### 3.1.2 Results for the $\sqrt{s}_{\max} = 7$ TeV Ensemble

Here, we consider as initial values each one of the corresponding results obtained with the  $\sqrt{s}_{\max} = 1.8$  TeV ensemble, namely, those listed in Table 1. The numerical results and statistical information are displayed in Table 2.

The corresponding curves obtained with method 1 for both ensembles and the experimental data are shown in Figs. 1, 2, 3, and 4. In each figure, the COMPETE result is displayed as reference (solid lines), together with each result obtained with ensembles  $\sqrt{s}_{\max} = 1.8$  TeV (dot-dashed lines) and  $\sqrt{s}_{\max} = 7$  TeV (dotted lines): direct fit and variants 1, 2, and 3 in Figs. 1, 2, 3, and 4, respectively.

In these figures, the estimates for the total cross section from cosmic-ray experiments at the highest energies were also displayed, which were not included in the data reductions. These estimates, discussed in [47] (see also [48]), were obtained by the Akeno Collaboration [56] in the  $\sim 6$ –24 TeV region, and by the Fly's Eye Collaboration at 30 TeV [57]. Also included is the recent result by the Pierre Auger Collaboration at 57 TeV [58]. We shall discuss these and the results that follows in Section 4.

## 3.2 Method 2

### 3.2.1 Results for the $\sqrt{s}_{\max} = 1.8$ TeV Ensemble

The initial values, referred to in the beginning of this section, are displayed in the second column of Table 3. Here, the following variants have been considered:

**Variant 4 (V4):** The parameters  $b_1$  and  $b_2$  have been fixed to the average values expected for the Reggeon intercepts and  $\gamma = 2$  is also fixed (third column of Table 3).

**Table 2** Results of method 1 for the  $\sqrt{s}_{\max} = 7$  TeV ensemble

	Direct fit	V1	V2	V3
$a_1$	$54.9 \pm 5.3$	$57.7 \pm 2.0$	$53.8 \pm 3.0$	$58.4 \pm 2.4$
$b_1$	$0.539 \pm 0.080$	$0.526 \pm 0.010$	0.452 (fixed)	0.452 (fixed)
$a_2$	$33.2 \pm 2.3$	$33.2 \pm 1.7$	$35.77 \pm 0.36$	$35.78 \pm 0.36$
$b_2$	$0.541 \pm 0.016$	$0.541 \pm 0.012$	0.558 (fixed)	0.558 (fixed)
$\alpha$	$35.9 \pm 1.9$	$34.90 \pm 0.23$	$32.68 \pm 0.87$	$30.41 \pm 1.00$
$\beta$	$0.290 \pm 0.027$	$0.199 \pm 0.014$	$0.257 \pm 0.017$	$0.093 \pm 0.019$
$\gamma$	2 (fixed)	$2.104 \pm 0.027$	2 (fixed)	$2.273 \pm 0.039$
$s_h$	$26 \pm 20$	$11.0 \pm 1.4$	$7.8 \pm 3.5$	$0.77 \pm 0.58$
DOF	157	156	159	158
$\chi^2/\text{DOF}$	0.930	0.935	0.931	0.933

Fit results with initial values corresponding to the final values given in Table 1: direct fit and variants 1, 2, and 3. Units as in Table 1

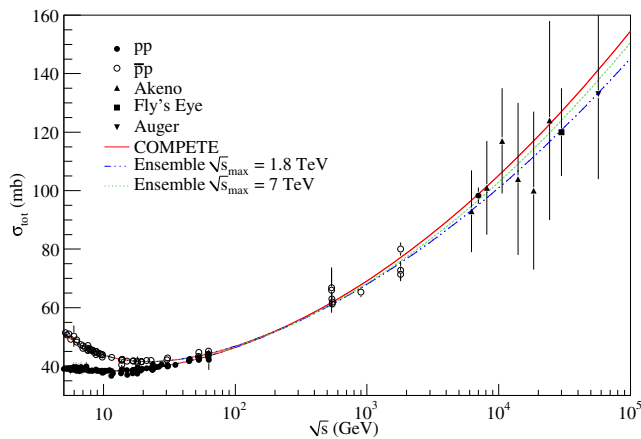


**Fig. 2** (Color online) Analogous to Fig. 1, the *dot-dashed* and *dotted* lines computed with variant 1 of method 1 (V1). Numerical information are displayed in Tables 1 (fourth column) and 2 (third column)

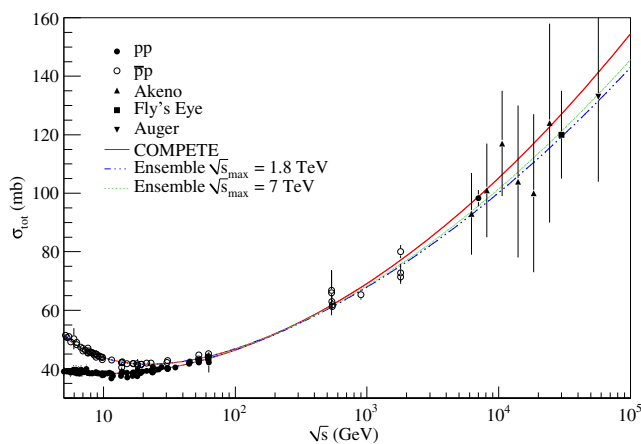


**Fig. 3** (Color online) Analogous to Fig. 1, the *dot-dashed* and *dotted* lines computed with variant 2 of method 1 (V2). Numerical information are displayed in Tables 1 (fifth column) and 2 (fourth column)

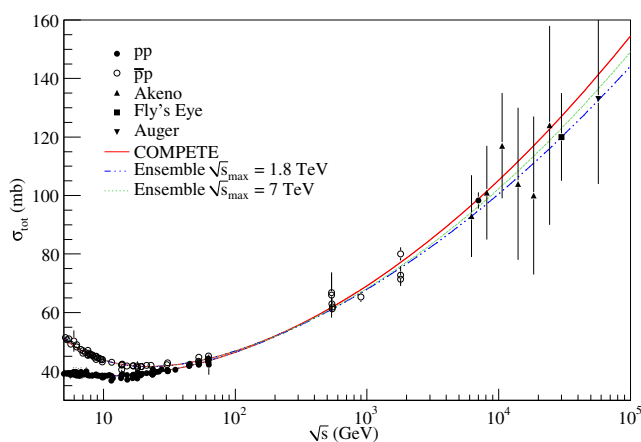


**Fig. 4** (Color online) Analogous to Fig. 1, the *dot-dashed* and *dotted* lines computed with variant 3 of method 1 (V3). Numerical information are displayed in Tables 1 and 2 (last columns)

**Table 3** Results of method 2 for the  $\sqrt{s}_{\max} = 1.8$  TeV ensemble

	Initial values	V4	V5	V6
$a_1$	1	$52.6 \pm 3.4$	$54.7 \pm 2.6$	$53.8 \pm 1.8$
$b_1$	0.5	0.5 (fixed)	0.5 (fixed)	$0.4952 \pm 0.0099$
$a_2$	1	$27.70 \pm 0.28$	$27.71 \pm 0.28$	$33.1 \pm 1.7$
$b_2$	0.5	0.5 (fixed)	0.5 (fixed)	$0.540 \pm 0.012$
$\alpha$	1	$34.86 \pm 0.69$	$34.32 \pm 0.77$	$34.60 \pm 0.24$
$\beta$	50	$0.270 \pm 0.019$	$0.21 \pm 0.11$	$0.290 \pm 0.021$
$\gamma$	2	2 (fixed)	$2.06 \pm 0.16$	$1.975 \pm 0.028$
$s_h$	1	$15.6 \pm 6.3$	$9.3 \pm 8.4$	$16.0 \pm 2.0$
DOF	–	158	157	155
$\chi^2/\text{DOF}$	–	0.963	0.969	0.937

Fit results with Variants 4, 5, and 6. Units as in Table 1

**Table 4** Results of method 2 for the  $\sqrt{s}_{\max} = 7$  TeV ensemble

	V4	V5	V6
$a_1$	$51.34 \pm 3.2$	$56.5 \pm 1.1$	$57.6 \pm 7.5$
$b_1$	0.5 (fixed)	0.5 (fixed)	$0.525 \pm 0.077$
$a_2$	$27.70 \pm 0.28$	$27.70 \pm 0.28$	$33.2 \pm 2.3$
$b_2$	0.5 (fixed)	0.5 (fixed)	$0.541 \pm 0.016$
$\alpha$	$35.13 \pm 0.60$	$33.65 \pm 0.22$	$34.9 \pm 1.7$
$\beta$	$0.279 \pm 0.016$	$0.1301 \pm 0.0086$	$0.199 \pm 0.064$
$\gamma$	2 (fixed)	$2.213 \pm 0.024$	$2.10 \pm 0.11$
$s_h$	$18.5 \pm 6.3$	$3.90 \pm 0.52$	$10.8 \pm 5.6$
DOF	159	158	156
$\chi^2/\text{DOF}$	0.962	0.967	0.935

Fit results with variants 4, 5, and 6. Same units as in Table 1

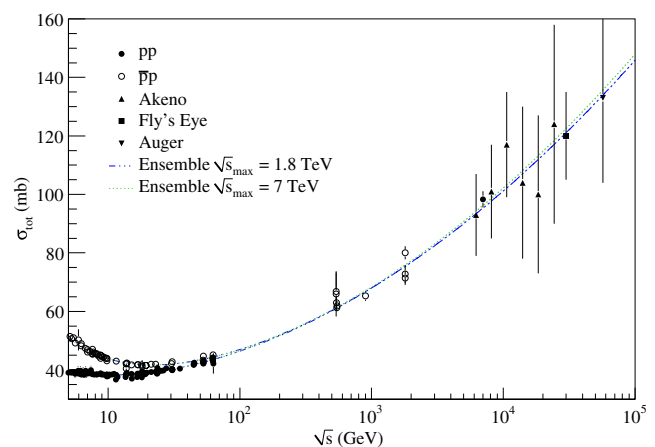


**Fig. 5** (Color online) Analogous to Fig. 1, the *dot-dashed* and *dotted* lines computed with variant 4 of method 2 (V4). Numerical information are displayed in Tables 3 (third column) and 4 (second column)

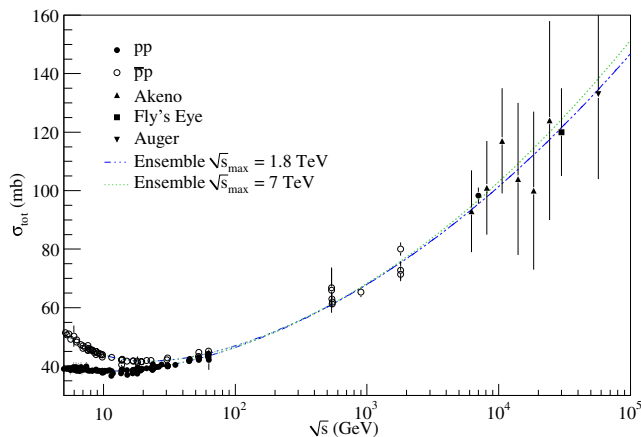


**Fig. 6** (Color online) Analogous to Fig. 1, the *dot-dashed* and *dotted* lines computed with variant 5 of method 2 (V5). Numerical information are displayed in Tables 3 (fourth column) and 4 (third column)

**Variant 5 (V5):** Same as variant 4 with  $\gamma$  as free parameter (fourth column of Table 3).

**Variant 6 (V6):** Initialized with the parameters from variant 4;  $b_1$ ,  $b_2$ , and  $\gamma$  free parameters (fifth column of Table 3).

The following diagram summarizes the fit procedures and initial values (Table 3):

Initial Values  $\rightarrow$   $\begin{cases} \text{Variant 4} \rightarrow \text{Variant 6} \\ \text{Variant 5} \end{cases}$

### 3.2.2 Results for the $\sqrt{s}_{\text{max}} = 7$ TeV Ensemble

Here, we followed the same procedure described above, now with the expanded ensemble. Table 4 dis-

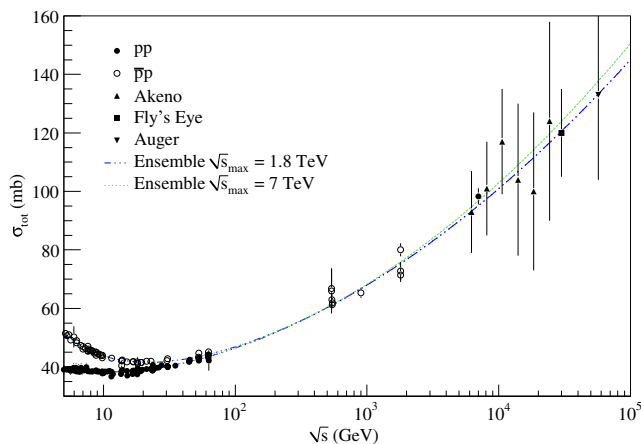


**Fig. 7** (Color online) Analogous to Fig. 1, the *dot-dashed* and *dotted* lines computed with variant 6 of method 2 (V6). Numerical information are displayed in Tables 3 (fifth column) and 4 (fourth column)

plays the numerical results and statistical information. Figures 5, 6, and 7 compare the accelerator data and estimates from cosmic-ray experiments with the fits obtained with method 2 and variants 4, 5, and 6, respectively, for the  $\sqrt{s}_{\text{max}} = 1.8$  TeV (dot-dashed lines) and  $\sqrt{s}_{\text{max}} = 7$  TeV (dotted lines) ensembles.

We note a difference in the diagrams related to initial values and variants (two schemes displayed in this section). This effect is a consequence of fit procedures since in certain cases, the data reductions led back to the initial values or to solutions with errors that exceeded the central values of the parameters. All these cases have been excluded.

## 4 Conclusions and Final Remarks

We have employed two methods to initialize the fitting parameters, six variants and two data ensembles. The results for the  $\sqrt{s}_{\text{max}} = 1.8$  TeV ensemble, listed in Tables 1 and 3, are statistically consistent with  $\gamma = 2$ , which points to a saturation of the squared logarithm dependence for the total cross section at high energies. More specifically, the results can be summarized as follows:

Method 1 (Table 1):

$$\gamma \approx 2.00 \pm 0.03 \quad (\text{V1}) \quad \text{and} \quad \gamma \approx 2.08 \pm 0.10 \quad (\text{V3}).$$

Method 2 (Table 3):

$$\gamma \approx 2.06 \pm 0.16 \quad (\text{V5}) \quad \text{and} \quad \gamma \approx 1.98 \pm 0.03 \quad (\text{V6}).$$

On the other hand, when the more recent 7-TeV TOTEM datum is included, all fits with  $\gamma$  as a free parameter, listed in Tables 2 and 4, are statistically consistent with exponents above 2, as indicated in the following summary:

Method 1 (Table 2):

$$\gamma \approx 2.10 \pm 0.03 \quad (\text{V1}) \quad \text{and} \quad \gamma \approx 2.27 \pm 0.04 \quad (\text{V3}).$$

Method 2 (Table 4):

$$\gamma \approx 2.21 \pm 0.02 \quad (\text{V5}) \quad \text{and} \quad \gamma \approx 2.10 \pm 0.11 \quad (\text{V6}).$$

All these results for  $\gamma$ , together with those obtained by Amaldi et al. and the UA/4 Collaboration, are schematically displayed in Fig. 8. From our data reductions through parametrization (3–5) to pp and  $\bar{p}p$  scattering above 5 GeV, including the 7-TeV TOTEM result, we conclude that the total hadronic cross section may rise faster than  $\ln^2 s$  at high energies.

From Fig. 8, we see that the central values of the  $\gamma$  parameter from the fits with  $\sqrt{s}_{\text{max}} = 1.8$  TeV (methods

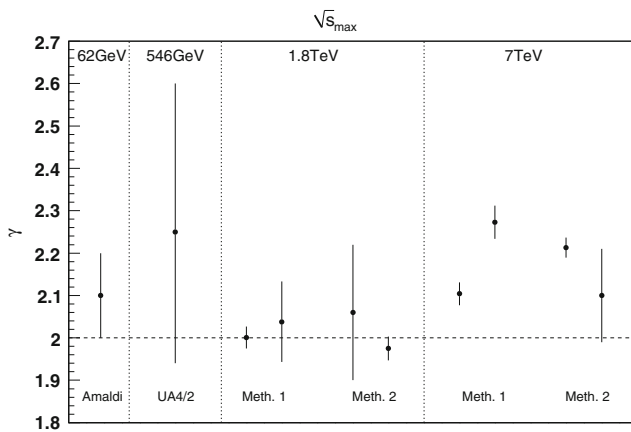


**Fig. 8** Results for the exponent  $\gamma$  as a free parameter in different data reductions through parametrization (3–5). Shown are the results by Amaldi et al. [30] ( $\sqrt{s}_{\max} = 62$  GeV), the UA4/2 Collaboration [31] ( $\sqrt{s}_{\max} = 546$  GeV), and from our analyses for the  $\sqrt{s}_{\max} = 1.8$  TeV and  $\sqrt{s}_{\max} = 7$  TeV ensembles with methods 1 and 2

1 and 2) are below the corresponding values obtained by Amaldi et al. and by the UA4/2 Collaboration. Since these authors have included the  $\rho$  information in their analysis, it seems not clear that simultaneous fits to  $\rho$  and  $\sigma_{\text{tot}}$  data may, in that case, anchor the rise of the total cross section. In other words, we understand that the results we have obtained with  $\sqrt{s}_{\max} = 1.8$  TeV and  $\sqrt{s}_{\max} = 7$  TeV ensembles are not connected with the inclusion or not of the  $\rho$  information but are direct consequences of the total cross-section data analyzed and the possibility to treat  $\gamma$  as a free fit parameter (not fixed to 2). In fact, our *predictions* for  $\rho(s)$  in the case of  $\gamma > 2$  are presented in the [Appendix](#) and show good agreement with experimental information available above 5 GeV.

Concerning the rise of the total cross section faster than the squared logarithm dependence, we have the following final comments:

1. In the theoretical context, different assumptions on the nonphysical amplitudes in the asymptotic region can explain this behavior, which does not mean violation of unitarity, as recently discussed by Azimov [18].
2. In the experimental context, beyond the LHC energy region, extremely large uncertainties are associated with estimations of the pp total cross section from cosmic-ray experiments. Such uncertainties are unavoidable since the flux decreases as the energy grows and because the extraction of  $\sigma_{\text{pp}}$  from  $\sigma_{\text{p-air}}$  is model dependent. These estimations have been included in our figures for qualitative comparison only. It may be useful to recall that the

results of the Akeno Collaboration [56] have been criticized in several works, as discussed for example in Refs. [25] and [47], and references therein. Had we ignored this information, the Fly's Eye and Auger results, i.e., the highest energy points in our figures, might suggest a different scenario for the rise of the total cross section. In fact, from Figs. 1, 2, 3, 4, 5, 6, and 7, all the curves which are consistent with the TOTEM point lie above the central values of these cosmic-ray estimations and the same is true in the inverse sense. That is, *there is no agreement among the TOTEM result and the Fly's Eye and Auger estimations, at least in what concerns parametrization (3–5)*. In this sense, the expected measurement of  $\sigma_{\text{tot}}$  by the TOTEM Collaboration at 7 and 8 TeV through the luminosity-independent [6, 9] method may shed light on the subject. Moreover, new experimental results on elastic and diffractive scattering at 8 TeV (and, subsequently, at 14 TeV) will provide novel phenomenological insights and reduce the uncertainties from model extrapolations necessary to obtain  $\sigma_{\text{tot}}$  from cosmic-ray experiments (see [59] and references therein).

At last, we stress that our approach and strategies do not follow the usual or standard lines of the amplitude analyses on the energy dependence of the total cross section. As commented, the latter include  $\rho$  data, associate the parametrization with data at low energies, and constrain the fits to describe other reactions, for which low-energy data are available. These are aspects that we expect to consider in a future work, since they may provide information that is complementary to the results we have presented. As commented along the manuscript, our goal has been to explore the possibility of investigating only the reactions with the highest energy interval available, concentrating on the total cross-section data. We have tried to identify possible high-energy effects that may be unrelated to the trends of the lower energy data (including those from other reactions) or hidden in fits including the  $\rho$  information. Our intention is not to compete with other authors or analysis, but to call the attention to the possibility that the rise of the total hadronic cross section may still constitute an open problem, an assertion that contrasts with the view advocated by some authors [28].

*Note Added During Revision* After this paper was submitted to publication, new fits of forward quantities were obtained by the Particle Data Group [60]. The updated data set includes the TOTEM result at 7 TeV and the new fit with the highest rank COMPETE parametrization ( $\gamma = 2$ ) shows that the point at 7 TeV is not

described: the curve lies below the data (Fig. 46.10 in [60]). This result corroborates those that were already shown with the  $\sqrt{s}_{\max} = 7$  TeV ensemble in our Figs. 1, 3, and 5.

**Acknowledgements** We are thankful to an anonymous referee for valuable comments. This research was supported by the FAPESP under contracts 11/15016-4, 11/00505-0 and 09/50180-0.

## Appendix: Predictions for the Ratio Between the Real and Imaginary Parts of the Forward Amplitude

In this appendix, we present predictions for  $\rho(s)$  from fits to pp and  $\bar{p}p$  total cross-section data through parametrization (3–5) with  $\gamma > 2$ . We also discuss the effect and role of the subtraction constant, embodied in the associated dispersion relation. In search of extreme effects, we shall consider the two results obtained with the  $\sqrt{s}_{\max} = 7$  TeV ensemble, which correspond to the highest exponents  $\gamma$ , namely,

Method 1—Variant 3:  $\gamma \approx 2.27 \pm 0.04$  (Table 2)

Method 2—Variant 5:  $\gamma \approx 2.21 \pm 0.02$  (Table 4)

In terms of the *forward* scattering amplitude  $F(s)$ , the total cross section (optical theorem) and the ratio between the real and imaginary parts of the amplitude, at high energies, can be expressed by

$$\sigma_{\text{tot}}(s) = \frac{\text{Im } F(s)}{s}, \quad \rho(s) = \frac{\text{Re } F(s)}{\text{Im } F(s)}. \quad (6)$$

For crossing even (+) and odd (−) amplitudes, pp and  $\bar{p}p$  scattering are related by

$$F_{\pm}(s) = \frac{F_{\text{pp}} \pm F_{\bar{p}p}}{2} \quad (7)$$

and it follows from (6) and (7) that

$$\rho^{\text{pp}} = \frac{1}{\sigma_{\text{tot}}^{\text{pp}}(s)} \left\{ \frac{\text{Re } F_+}{s} + \frac{\text{Re } F_-}{s} \right\} \quad (8)$$

and

$$\rho^{\bar{p}p} = \frac{1}{\sigma_{\text{tot}}^{\bar{p}p}} \left\{ \frac{\text{Re } F_+}{s} - \frac{\text{Re } F_-}{s} \right\}. \quad (9)$$

The real and imaginary parts of the even and odd amplitudes are connected by dispersion relations and the high-energy domain demands one subtraction [45, 46]. Since we are looking for analytical results, we shall work here with the derivative dispersion relations in the

standard form deduced by Bronzan et al. [61]. They are obtained from the integral dispersion relations in the high-energy limit:

$$\frac{\text{Re } F_+(s)}{s} = \frac{K}{s} + \tan \left[ \frac{\pi}{2} \frac{d}{d \ln s} \right] \frac{\text{Im } F_+(s)}{s},$$

$$\frac{\text{Re } F_-(s)}{s} = \tan \left[ \frac{\pi}{2} \left( 1 + \frac{d}{d \ln s} \right) \right] \frac{\text{Im } F_-(s)}{s}.$$

where  $K$  is the *subtraction constant*. Operationally, these relations can be evaluated through the expansions [62, 63]

$$\begin{aligned} \frac{\text{Re } F_+(s)}{s} - \frac{K}{s} &= \left[ \frac{\pi}{2} \frac{d}{d \ln s} + \frac{1}{3} \left( \frac{\pi}{2} \frac{d}{d \ln s} \right)^3 \right. \\ &\quad \left. + \frac{2}{15} \left( \frac{\pi}{2} \frac{d}{d \ln s} \right)^5 + \dots \right] \frac{\text{Im } F_+(s)}{s}, \end{aligned} \quad (10)$$

$$\begin{aligned} \frac{\text{Re } F_-(s)}{s} &= - \int \left\{ \frac{d}{d \ln s} \left[ \cot \left( \frac{\pi}{2} \frac{d}{d \ln s} \right) \right] \frac{\text{Im } F_-(s)}{s} \right\} d \ln s \\ &= - \frac{2}{\pi} \int \left\{ \left[ 1 - \frac{1}{3} \left( \frac{\pi}{2} \frac{d}{d \ln s} \right)^2 \right. \right. \\ &\quad \left. \left. - \frac{1}{45} \left( \frac{\pi}{2} \frac{d}{d \ln s} \right)^4 - \dots \right] \right. \\ &\quad \left. \times \frac{\text{Im } F_-(s)}{s} \right\} d \ln s. \end{aligned} \quad (11)$$

With parametrization (3–5) taken as input, a closed form results from the sum of the contributions associated with the power-law term  $\sigma_{\text{LE}}$ . The sum of the contributions from the logarithm term  $\sigma_{\text{HE}}$  converges fast for  $\gamma$  in the range (2.2–2.3) and a third-order approximation is therefore sufficient. We obtain for the even part

$$\begin{aligned} \frac{\text{Re } F_+(s)}{s} &= \frac{K}{s} - a_1 \tan \left( \frac{\pi b_1}{2} \right) \left[ \frac{s}{s_l} \right]^{-b_1} + A \ln^{\gamma-1} \left( \frac{s}{s_h} \right) \\ &\quad + B \ln^{\gamma-3} \left( \frac{s}{s_h} \right) + C \ln^{\gamma-5} \left( \frac{s}{s_h} \right), \end{aligned} \quad (12)$$

where

$$\begin{aligned} A &= \frac{\pi}{2} \beta \gamma, & B &= \frac{1}{3} \left[ \frac{\pi}{2} \right]^3 \beta \gamma [\gamma - 1][\gamma - 2], \\ C &= \frac{2}{15} \left[ \frac{\pi}{2} \right]^5 \beta \gamma [\gamma - 1][\gamma - 2][\gamma - 3][\gamma - 4] \end{aligned} \quad (13)$$

and for the odd part

$$\frac{\text{Re } F_{-}(s)}{s} = -a_2 \cot\left(\frac{\pi b_2}{2}\right) \left[\frac{s}{s_l}\right]^{-b_2}. \quad (14)$$

With the above results, (8) and (9) yield analytical expressions for  $\rho^{\text{pp}}(s)$  and  $\rho^{\bar{\text{p}}\text{p}}(s)$ . Note that the analytical results imply that as  $s \rightarrow \infty$ ,

$$\rho \propto 1/\ln s \rightarrow 0.$$

In what follows, we present the predictions for  $\rho(s)$  and compare the results with the experimental information available [10]. To study the effect of the subtraction constant, we follow two alternatives: in the first, we fix it at  $K = 0$ ; in the second, we let  $K$  be a fit parameter to the  $\rho$  data only. More specifically, we take as input the parameters in Tables 2 and 4, with  $s_l = 1 \text{ GeV}^2$ .

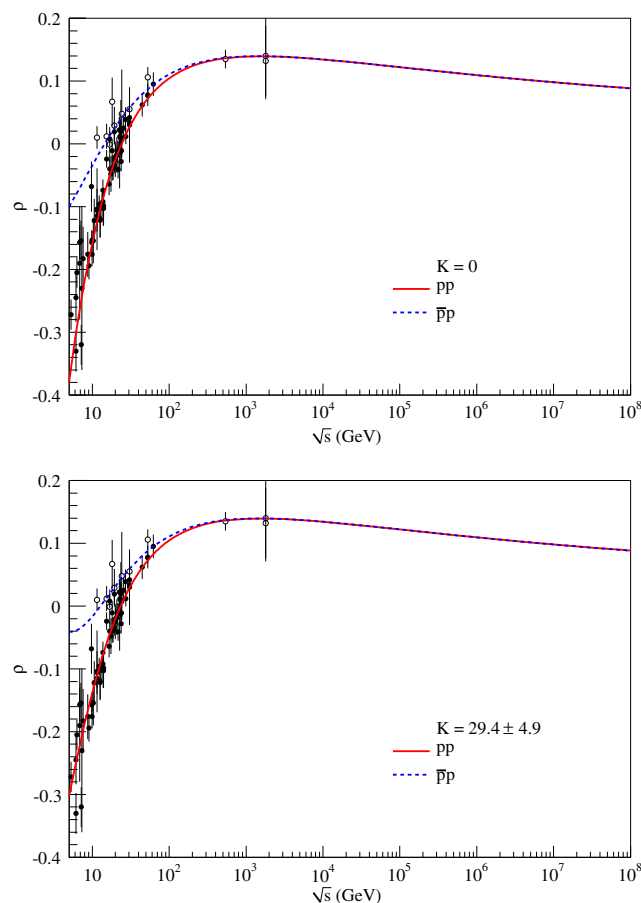


**Fig. 9** (Color online) Comparison between experimental results for  $\rho$  and the analytical expressions derived in the Appendix, with the parameters obtained by variant 3 of method 1, listed in Table 2, which yield  $\gamma \approx 2.27 \pm 0.04$ . The filled and the open circles represent the experimental data for pp and  $\bar{\text{p}}\text{p}$  scattering, respectively. The top panel shows our predictions with  $K = 0$ , which correspond to  $\chi^2/\text{DOF} = 1.93$ . The bottom panel is the best fit to the  $\rho$  data with  $K$  a free parameter ( $\chi^2/\text{DOF} = 1.45$ )

In the first alternative,  $K = 0$ , we obtain the direct prediction for  $\rho(s)$ . In the second alternative, we fix all the other parameters and adjust  $K$  to fit the  $\rho$  data. In the latter case, the first run of the MINUIT Code yields the  $\chi^2/\text{DOF}$  for  $K = 0$ . The predictions with the results by method 1—variant 3 (Table 2) are displayed in Fig. 9 and those with the results by method 2—variant 5 (Table 4) are in Fig. 10. We are led to the following conclusions:

1. Even in these extrema cases, with  $\gamma : 2.2 - 2.3$ , all the experimental information on  $\rho^{\text{pp}}(s)$  and  $\rho^{\bar{\text{p}}\text{p}}(s)$  above 5 GeV are quite well described;
2. The subtraction constant affects the low-energy results, below  $\sqrt{s} \sim 20 \text{ GeV}$ ;
3. The best  $\chi^2/\text{DOF}$  results (closest to 1) are obtained with  $K$  as a free fit parameter. Obviously, that is a consequence of adding one more free parameter,

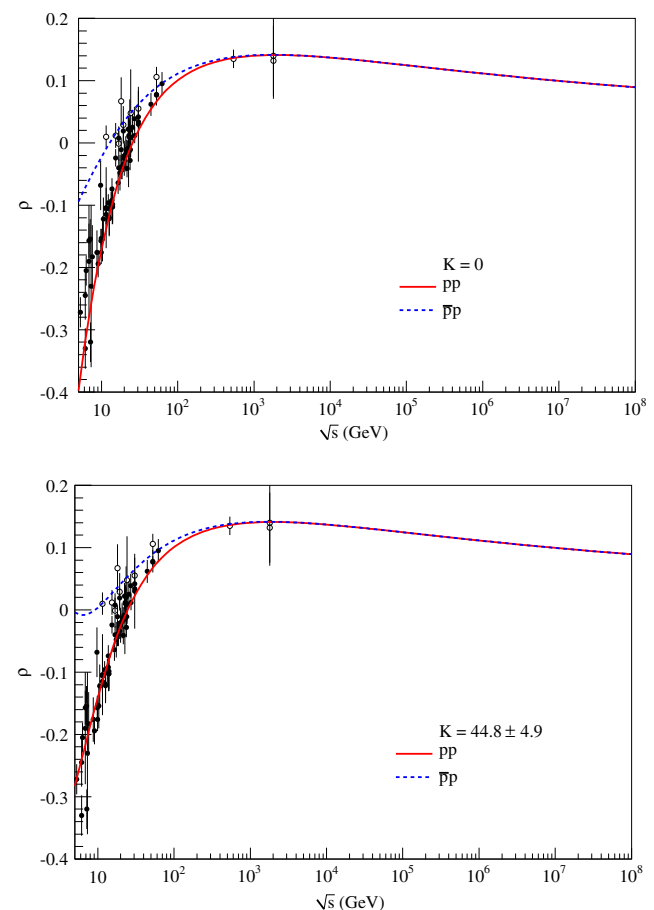


**Fig. 10** (Color online) Analogous to Fig. 9, the analytical results were plotted for the parameters obtained with variant 5 of method 2 (Table 4), which yield  $\gamma \approx 2.21 \pm 0.02$ . The ratios  $\chi^2/\text{DOF}$  in the top and bottom panels are 2.70 and 1.58, respectively

however, without the physical interpretation associated with those present in the parametrization of the total cross section.

Finally, we recall that in simultaneous fits to  $\sigma_{\text{tot}}$  and  $\rho$ , the subtraction constant affects both the low- and high-energy regions [47, 48]. That is a consequence of the strong correlation among the subtraction constant and all the other physical free fit parameters. We plan to discuss this consequence and other aspects of the fit procedures in a forthcoming paper.

## References

1. D.H. Perkins, *Introduction to High Energy Physics*, 4th edn. (Cambridge University Press, Cambridge, 2000)
2. W. Greiner, S. Schramm, E. Stein, *Quantum Chromodynamics*, 3rd edn. (Springer, Berlin, 2007)
3. F. Halzen, A.D. Martin, *Quarks & Leptons: an Introductory Course in Modern Particle Physics* (Wiley, New York, 1984)
4. R.D. Field, *Applications of Perturbative QCD* (Addison-Wesley, Reading, 1989)
5. T. Muta, *Foundations of Quantum Chromodynamics* (World Scientific, Singapore, 1987)
6. V. Barone, E. Predazzi, *High-Energy Particle Diffraction* (Springer, Berlin, 2002)
7. S. Donnachie, G. Dosch, P.V. Landshoff, O. Natchmann, *Pomeron Physics and QCD* (Cambridge University Press, Cambridge, 2002)
8. E. Merzbacher, *Quantum Mechanics*, 3rd edn. (Wiley, New York, 1998)
9. G. Matthiae, Rep. Prog. Phys. **57**, 743 (1994)
10. K. Nakamura et al., (Particle Data Group), J. Phys. G **37**, 075021 (2010)
11. J. Kašpar, V. Kandrát, M. Lokajíček, J. Procházka, Nucl. Phys. B **843**, 84 (2011)
12. R. Fiore, L. Jenkovsky, R. Orava, E. Predazzi, A. Prokudin, O. Selyugin, Int. J. Mod. Phys. A **24**, 2551 (2009)
13. M. Froissart, Phys. Rev. **123**, 1053 (1961)
14. A. Martin, Nuovo Cimento A **42**, 930 (1966)
15. L. Lukaszuk, A. Martin, Nuovo Cim. A **52**, 122 (1967)
16. A. Martin, AIP Conf. Proc. **1105**, 258 (2009)
17. T.T. Wu, A. Martin, S.M. Roy, V. Singh, Phys. Rev. D **84**, 025012 (2011)
18. Y.I. Azimov, Phys. Rev. D **84**, 056012 (2011)
19. J.R. Cudell, K. Kang, S.K. Kim, Phys. Lett. B **395**, 311 (1997)
20. E.G.S. Luna, M.J. Menon, Phys. Lett. B **565**, 123 (2003)
21. K. Igi, M. Ishida, Phys. Rev. D **66**, 034023 (2002)
22. K. Igi, M. Ishida, Phys. Lett. B **622**, 289 (2005)
23. M. Ishida, K. Igi, Prog. Theor. Phys. Suppl. **187**, 297 (2011)
24. J.R. Cudell et al., (COMPETE Collaboration), Phys. Rev. Lett. **89**(20), 201801 (2002)
25. J.R. Cudell et al., (COMPETE Collaboration), Phys. Rev. D **65**, 074024 (2002)
26. M.M. Block, F. Halzen, Phys. Rev. D **70**, 091901 (2004)
27. M.M. Block, F. Halzen, Phys. Rev. D **72**, 036006 (2005)
28. M.M. Block, F. Halzen, Phys. Rev. Lett. **107**, 212002 (2011)
29. G. Antchev et al., (TOTEM Collaboration), Europhys. Lett. **96**, 21002 (2011)
30. U. Amaldi et al., Phys. Lett. B **66**, 390 (1977)
31. C. Augier et al., (UA4/2 Collaboration), Phys. Lett. B **315**, 503 (1993)
32. M. Giordano, E. Meggiolaro, N. Moretti, Asymptotic energy dependence of hadronic total cross sections from lattice QCD, [arXiv:1203.0961](https://arxiv.org/abs/1203.0961)[hep-ph]
33. V.N. Gribov, A.A. Migdal, Sov. Phys. JETP **28**, 784 (1969)
34. M.G. Ryskin, A.D. Martin, V.A. Khoze, Diffractive processes at the LHC, in Gribov-75 Memorial Workshop, Budapest, 2005, [arXiv:hep-ph/0506272v1](https://arxiv.org/abs/hep-ph/0506272v1) (2005)
35. A. Grau, R.M. Godbole, G. Panzeri, Y.N. Srivastava, Phys. Lett. B **682**, 55 (2009)
36. A. Achilli, Y. Srivastava, R. Godbole, A. Grau, G. Panzeri, O. Shekhovtsova, Phys. Rev. D **84**, 094009 (2011)
37. R.J. Eden, *High Energy Collisions of Elementary Particles* (Cambridge University Press, Cambridge, 1967), Sect. 7.1.
38. M.M. Block, R.N. Cahn, Rev. Mod. Phys. **57**, 563 (1985)
39. M.M. Block, Phys. Rep. **436**, 71 (2006)
40. E. Martynov, J.R. Cudell, O.V. Selyugin, Eur. Phys. J. C **33**, S533 (2004)
41. E. Martynov, J.R. Cudell, O.V. Selyugin, Ukrainian J. Phys. **48**, 1274 (2003)
42. R.F. Ávila, M.J. Menon, Braz. J. Phys. **37**, 358 (2007)
43. R.F. Ávila, M.J. Menon, Extended derivative dispersion relations, in *Sense of Beauty in Physics - A Volume in Honour of Adriano Di Giacomo*, ed. by M. D'Elia et al. (Edizioni Plus—Pisa University Press, Pisa, Italy, 2006) pp. 153–158, [arXiv:hep-ph/0601194](https://arxiv.org/abs/hep-ph/0601194)
44. E. Ferreira, J. Sesma, J. Math. Phys. **49**, 033504 (2008)
45. M.L. Goldberger, Y. Nambu, R. Oehme, Ann. Phys. (NY) **2**, 226 (1957)
46. P. Söding, Phys. Lett. **8**, 285 (1964)
47. R.F. Ávila, E.G.S. Luna, M.J. Menon, Phys. Rev. D, **67**, 054020 (2003)
48. R.F. Ávila, E.G.S. Luna, M.J. Menon, Braz. J. Phys. **31**, 567 (2001).
49. E. Ferreira, Int. J. Mod. Phys. E **16**, 2893 (2007)
50. A.K. Kohara, E. Ferreira, T. Kodama, in *Proceedings of the 13th International Conference on Elastic and Diffractive Scattering*, CERN, 2009, ed. by M. Deile, D. d'Enterria, A. De Roeck (DESY, Hamburg, 2010) p. 12
51. A.K. Kohara, E. Ferreira, T. Kodama, in *XI HADRON PHYSICS, Maresias, 2010*, ed. by M. Nielsen, F.S. Navarra, M.E. Bracco, AIP Conference Proceedings 1296 (AIP, Melville, 2010) p. 270
52. C. Bourrely, J. Soffer, T.T. Wu, Eur. Phys. J. C **71**, 1601 (2011)
53. V. Kandrát, M. Lokajíček, I. Vrkoč, Phys. Lett. B **656**, 182 (2007)
54. P.R. Bevington, D.K. Robinson, *Data Reduction and Error Analysis for the Physical Sciences* (McGraw-Hill, Boston, 1992)
55. E.G.S. Luna, M.J. Menon, J. Montanha, Nucl. Phys. A **745**, 104 (2004)
56. M. Honda et al., Phys. Rev. Lett. **70**, 525 (1993)
57. R.M. Baltrusaitis et al., Phys. Rev. Lett. **52**, 1380 (1984)
58. P. Abreu et al., (The Pierre Auger Collaboration), Phys. Rev. Lett. **109**, 062002 (2012)
59. D.A. Fagundes, M.J. Menon, Nucl. Phys. A **880**, 1 (2012), [arXiv:1112.5115](https://arxiv.org/abs/1112.5115)[hep-ph]
60. J. Beringer et al., (Particle Data Group), Phys. Rev. D **86**, 010001 (2012), <http://pdg.lbl.gov>, Sect. 46. Plots of cross section and related quantities
61. J.B. Bronzan, G.L. Kane, U.P. Sukhatme, Phys. Lett. B **49**, 272 (1974)
62. K. Kang, B. Nicolescu, Phys. Rev. D **11**, 2461 (1975)
63. R.F. Ávila, M.J. Menon, Nucl. Phys. A **744**, 249 (2004)